

How to realize compact and Anderson-like localized states in disorder-free hypercube bosonic networks

Ievgen I. Arkhipov,¹ Fabrizio Minganti,^{2,3} and Franco Nori^{4,5,6}

¹*Joint Laboratory of Optics of Palacký University and Institute of Physics of CAS, Faculty of Science, Palacký University, 17. listopadu 12, 771 46 Olomouc, Czech Republic*

²*Laboratory of Theoretical Physics of Nanosystems (LTPN), Institute of Physics, École Polytechnique Fédérale de Lausanne (EPFL), 1015 Lausanne, Switzerland*

³*Center for Quantum Science and Engineering, École Polytechnique Fédérale de Lausanne (EPFL), CH-1015 Lausanne, Switzerland*

⁴*Theoretical Quantum Physics Laboratory, Cluster for Pioneering Research, RIKEN, Wako-shi, Saitama 351-0198, Japan*

⁵*Quantum Information Physics Theory Research Team,*

Quantum Computing Center, RIKEN, Wakoshi, Saitama, 351-0198, Japan

⁶*Physics Department, The University of Michigan, Ann Arbor, Michigan 48109-1040, USA*

(Dated: October 15, 2024)

We present a method to engineer various zero-energy localized states on disorder-free hypercube graphs. Previous works have already indicated that disorder is not essential for observing localization phenomena in noninteracting systems, with some prominent examples including the 1D Aubry-André model, characterized solely by incommensurate potentials, or 2D incommensurate Moiré lattices, which exhibit localization due to the flat band spectrum. Moreover, flat band systems with translational invariance can also possess so-called compact localized states, characterized by exactly zero amplitude outside a finite region of the lattice. Here we show that both compact and non-compact (i.e., Anderson-like) localized states can be observed on disorder-free hypercubes that can be constructed in a standard iterative manner via Cartan products. This construction also makes these localized states robust against perturbations. We illustrate and visualize our results on the example of an 8D hypercube projected on its Petrie polygon. Our findings can be readily tested on existing photonic experimental setups, where hypercube graphs studied can be emulated by bosonic networks of coupled optical cavities and/or waveguides, thus offering potential advancements in the development of various information and wave manipulation protocols.

I. INTRODUCTION

The disorder-induced localization phenomenon has been known since the seminal work of P. W. Anderson studying the quantum phase transition between an isolating and metallic phase [1]. In the presence of disorder, the wavefunction of electrons confined by one- and two-dimensional periodic potentials become exponentially localized in space, as multiple scattering processes generate destructive interference between the otherwise delocalized mode. In higher-dimensional disordered systems $D \geq 3$, there can coexist both extended and localized states, and the energy level separated these two is known as the mobility edge [2–6].

Disorder is not an essential ingredient for observing localization phenomena. For instance, localization can manifest in quasiperiodic systems without disorder, such as the 1D Aubry-André model, which is characterized by a quasiperiodic, i.e., incommensurate, potential energy [7, 8]. In 2D, the localization transition can occur in Moiré lattices [9], Vogel spirals [10], and in linear [11] or nonlinear quasicrystals [12]. Moreover, even in purely periodic, i.e., translational invariant, systems without quenched disorder, localization can arise due to many-body interactions. A primary example is the Mott transition from insulator to metal (superfluid) in fermionic (bosonic) systems, both demonstrated using ultracold gasses quantum simulators [13, 14], where the lo-

calization properties are rather triggered by the presence of Coulomb-like interactions. Furthermore, in 1D lattice gauge theories, localization can result from gauge superselection sectors that act as an effective internal quenched disorder [15, 16]. In 2D periodic systems, localization may occur due to emergent classical percolation transition that divides the system into isolated real-space clusters [17]. A form of localization can manifest also in non-interacting and periodic systems through the so-called compact localized states (CLSs), i.e., wavefunctions whose amplitude strictly vanishes outside a finite domain of a system. These CLSs emerge from destructive interference of macroscopically degenerate eigenstates whose existence is determined by a flat-band energy spectrum [18–24].

Apart from Hermitian systems, the localization phenomena can also be observed in disordered non-Hermitian systems as well [25, 26]. Additionally, it was found that the bulk-boundary correspondence failure in non-Hermitian systems is intrinsically related to the so-called non-Hermitian skin effect where a number of edge modes exponentially become localized at the boundaries [27–31]. These theoretical findings have been further experimentally validated in photonic platforms [32–34].

Here we investigate emerging and *controllable localization occurring in disorder-free systems* whose geometry is that of a hypercube graph. Similar hypercube struc-

tures have been studied in connection with various phenomena. In the classical realm, they are closely related to the mutation-selection models of population genetics, which seeks to predict gene susceptibility or resistance to mutations [35]. In the quantum field, hypercube structures and their spectral characteristics can be useful for evaluating geometric entanglement in multipartite states [36], for exhibiting phase-space features significantly smaller than Planck's constant [37], and even for implementing high-performance fault-tolerant quantum computing [38]. Hypercube geometry have also gained interest in condensed matter physics, particularly in the description of spin-glass models [39, 40]. Additionally, the spectral properties of chaotic hypercube lattices can bear resemblance to the Maldacena-Qi model, which describes wormholes [41]. Importantly, hypercubes with *disordered* potentials have been recently explored in the context of continuous parabolic Anderson models [42] and discrete models with quantum walks [43].

Specifically, we demonstrate that both zero-energy CLSs and non-compact localized states (NCLSs) can be engineered on hypercube graphs, which can be emulated by a bosonic network of coupled cavities or waveguides. The key difference between the two is that while CLSs have strictly zero amplitudes beyond a finite region in the lattice, NCLSs do not, making the latter more akin to Anderson localized states.

We show that in the case of identical site potentials, the hypercube spectrum exhibits macroscopic degenerate states, similar to those found in flat-band systems, whose destructive interference results in CLSs. This observation makes photonic hypercube graphs promising candidates for storing quantum information [21].

Conversely, (in)commensurate potentials can produce NCLSs with a controlled (single-site) periodic amplitude density. The NCLSs can thus be generated on a disorder-free hypercubes. This finding is in contrast to previous studies, e.g., Ref. [42], which attribute hypercube localization to disorder.

We describe a constructive procedure to obtain the parameters needed to generate these states, based on a recursive application of Cartan products to the basic building blocks of the hypercubes known as dions. This construction ensures that the engineered localized zero-energy states (ZESs) of the hypercube are robust against various perturbations and disorder.

Our findings can be directly verified on current photonic experimental setups [44–46]. This can enable advancements in the development of novel information and wave manipulation protocols.

This paper is structured as follows: In Sec. II, we give a brief summary of our main results on localization on hypercube graphs characterized by ordered site potentials. In Sec. III, we introduce and describe a general method for constructing hypercubes with certain ordered site potentials and outline its main properties. Section IV focuses on the applicability of this method for engineering CLSs on the example of 8D hypercubes. In Sec. V, we ex-

plore the construction of NCLSs with both single-site and periodic amplitude densities and their robustness against imposed disorder. Conclusions and outlook are provided in Sec. VI.

II. OVERVIEW OF THE MAIN RESULTS

In this work we focus on the study of the eigenvalue problem of a Hamiltonian

$$H\psi = E\psi, \quad (1)$$

which describes a certain disorder-free hypercube graph. Such a graph can emulate, e.g., a set of coupled waveguides or cavities. In that case the Hamiltonian H can be written in the mode representation, i.e., $\hat{H} = \hat{\Psi}^\dagger H \hat{\Psi}$, where $\hat{\Psi} = [\hat{a}_1, \dots, \hat{a}_n]^T$ is the vector of the bosonic annihilation operators, where an operator \hat{a}_j represents a mode j . The bosonic operators also obey the known commutation relations, namely, $[\hat{a}_j, \hat{a}_k] = 0$, and $[\hat{a}_j^\dagger, \hat{a}_k] = \delta_{jk}$, with δ_{jk} being a Kronecker delta function.

More specifically, a bosonic Hamiltonian defined on an n -dimensional hypercube graph can read as

$$\hat{H} = \sum_{i=1}^{2^n} \nu(i) \hat{a}_i^\dagger \hat{a}_i + g \left(\sum_{j,k \in \mathcal{N}_j} \hat{a}_j \hat{a}_k^\dagger + \text{h.c.} \right), \quad (2)$$

where $\nu(i)$ and g account for the potential energy (frequency) at the hypercube site i , and the nearest-neighbor site interaction energy, respectively, where \mathcal{N}_j is the set of n vertices constituting the nearest-neighbors of the site j . The potential energy here thus can be considered as the frequency of the mode \hat{a}_i , and the parameter g as the intermode coupling strength.

Our main result is that localization phenomena on such a bosonic hypercube graph, with constant intersite (intermode) coupling $g = 1$, can be observed and even controlled when the site potential attains the following ordered form:

$$\nu(i) = \sum_{j=1}^n \alpha_j \mathcal{H}(f_{i,j}) + \beta_j \mathcal{H}(-f_{i,j}), \quad (3)$$

where $f_{i,j} = \sin \left[2^j \pi i / (N - 1) \right]$, and $\mathcal{H}(x)$ denotes the Heaviside step function, i.e.,

$$\mathcal{H}(x) = \begin{cases} 1, & x \geq 0, \\ 0, & x < 0, \end{cases} \quad (4)$$

and α_j, β_j are, in general, certain real-valued coefficients dependent on the index j . Depending on the values of α_j, β_j the potential energy in Eq. (3) can display either constant, commensurate or incommensurate behavior, leading to the emergence of both compact and non-compact localized states in the hypercube eigenspectrum. Crucially, by demonstrating this, we reveal that *localization on a hypercube does not require the presence of disorder*, contrary to previous suggestions.

III. THEORY

A. Hypercube construction

We first set the stage by describing a general framework for hypercube construction and its spectral characteristics.

Geometrically, an n -dimensional hypercube can be readily constructed by iteratively applying the Cartesian product of n 1-dimensional edges (dions) [47, 48]. For instance, in 2D a Cartesian product of two dions generates a square; in 3D, three dions give a cube, and so on. The resulting n -cube has in total 2^n vertices and $2^{n-1}n$ edges. In a quantum mechanical formalism, the iterative Cartesian products of dions correspond to iterative Kronecker sums applied to the Hamiltonians that describe the dions. Specifically, we choose the description where each dion can be associated with a 2×2 matrix

$$S_k = \begin{pmatrix} \alpha_k & \kappa_k \\ \kappa_k & \beta_k \end{pmatrix} \quad (5)$$

representing the Hamiltonian of a qubit or that of a linear two-mode system. Following this choice, a $2^n \times 2^n$ Hamiltonian matrix H_n of weighted n -hypercube graph can be iteratively constructed. One fixes

$$H_1 = S_1 \quad (6)$$

and then

$$H_n = H_{n-1} \otimes I_2 + I_{n-1} \otimes S_n, \quad n > 1, \quad (7)$$

where I_k is the identity on the k -dimensional Hilbert space. Importantly, when $\alpha_k = \beta_k = 0$, and $\kappa_k = 1$, the Hamiltonian takes the form of an ordinary adjacency matrix of a regular n -hypercube with zero-potential vertices [49]. Throughout the text, without loss of generality, we assume $\kappa_k = 1 \forall k$.

In this regard, we note that previous studies on hypercube localization primarily began with hypercubes featuring zero-site potentials, where the diagonal elements were later perturbed in a *disordered* manner (see, e.g., Ref. [42]). In contrast, here we demonstrate that a more general construction of a weighted hypercube is sufficient to observe localization.

From Eq. (7) it directly follows that $N = 2^n$ vertices, or sites, of the n -dimensional hypercube with indices $i = 0, \dots, N - 1$ are characterized by the potentials

$$\nu(i) = \sum_{j=1}^n \alpha_j \mathcal{H}(f_{i,j}) + \beta_j \mathcal{H}(-f_{i,j}). \quad (8)$$

Note also that when $\nu(i) = 0$, the n -dimensional hypercube can be readily interpreted as a system of $2d$ interacting Majorana fermions [39, 41], or as the interaction term in the Maldacena-Qi model describing a space-time

wormhole [50]. Indeed, by introducing the gamma matrices

$$\begin{aligned} \gamma_k^L &= \begin{pmatrix} \otimes_{k-1} \sigma_x \\ 1 \end{pmatrix} \otimes \sigma_z \otimes I_{2^{n-2k}}, \\ \gamma_k^R &= \begin{pmatrix} \otimes_{k-1} \sigma_x \\ 1 \end{pmatrix} \otimes \sigma_y \otimes I_{2^{n-2k}}, \end{aligned} \quad (9)$$

with $\sigma_{x,y,z}$ being the Pauli matrices, the Hamiltonian in Eq. (7) can read as

$$H = i \sum_k^d \gamma_k^L \gamma_k^R. \quad (10)$$

In the case when on-site potentials attain the form as in Eq. (8), the left and right spaces in Eq. (10) become coupled. As a result, the corresponding Hamiltonian acquires a more complicated form. Alternatively, a general n -dimensional hypercube Hamiltonian in Eq. (7) can be associated with a network of 2^n coupled bosonic modes, whose frequencies are identified with potentials $\nu(i)$ [see also Eq. (2)]. Since we are mainly interested in the localization properties of the $2^n \times 2^n$ matrix H_n in Eq. (7), we assume that the hypercube Hamiltonian has the bosonic mode representation.

B. Hypercube Eigenspectrum and Symmetry

The eigenvectors ψ and eigenvalues λ of the Hamiltonian H_n in Eq. (7) are straightforwardly obtained as follows

$$\psi_{i_1, i_2, \dots, i_n} = \otimes_{k=1}^n \psi_{i_k}^{(k)}, \quad \lambda_{i_1, i_2, \dots, i_n} = \sum_{k=1}^n \lambda_{i_k}^{(k)} \quad (11)$$

where $\psi_{i_k}^{(k)}$ ($\lambda_{i_k}^{(k)}$) denotes the $i_k = 1, 2$, eigenvector (eigenvalue) of the matrix S_k in Eq. (7) [47, 48].

The eigenvectors in Eq. (11), thus, have a binary tree structure [49] (see also Fig. 1 in Ref. [48]). Note that whereas the eigenspectrum of the H_n has a tensor product structure, the underlying 2^n coupled bosonic modes, constituting the Hamiltonian, as in Eq. (2), can not be presented in the same manner.

The construction in Eq. (7) implies that a hypercube Hamiltonian H_n possesses a chiral symmetry (within an appropriate gauge)

$$H'_n = H_n - \bar{\nu} I_{2^n}, \quad (12)$$

where

$$\bar{\nu} = \frac{\max[\nu(i)] + \min[\nu(i)]}{2}, \quad (13)$$

with $\nu(i)$ given in Eq. (8), and I is the identity matrix. That is

$$\mathcal{C} H'_n \mathcal{C}^\dagger = -H'_n, \quad \mathcal{C} = \otimes_{i=1}^n \sigma_y, \quad \mathcal{C}^\dagger \mathcal{C} = \mathcal{C} \mathcal{C}^\dagger = \mathcal{C}^2 = I, \quad (14)$$

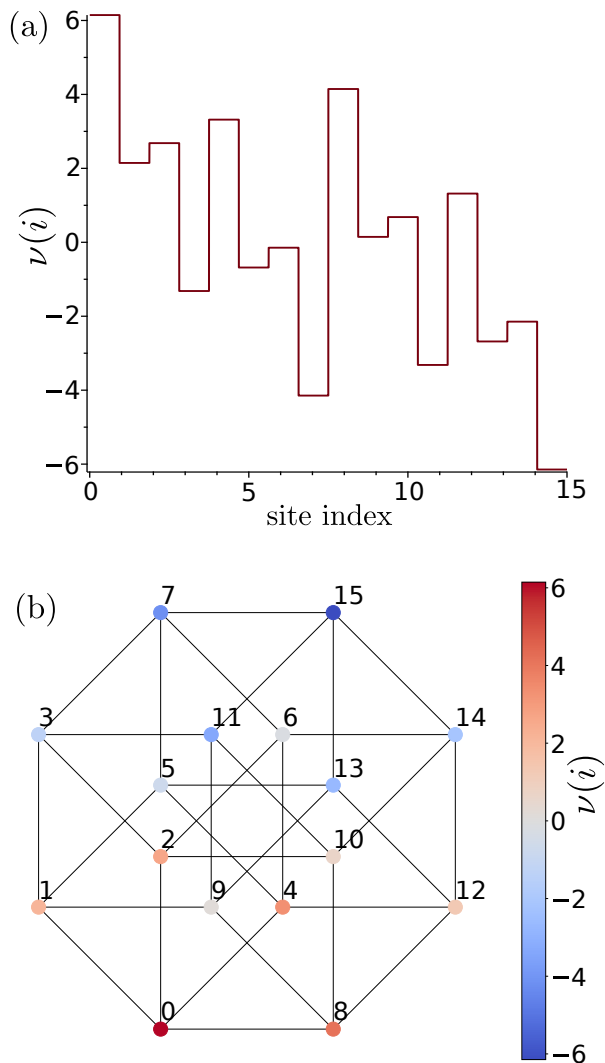


FIG. 1. (a) Site potentials $\nu(i)$ on a 4D hypercube described by the Hamiltonian in Eq. (7) generated by the dion matrices S_k , $k = 1, \dots, 4$, with diagonal elements $\alpha_k = -\beta_k = \sqrt{k}$. (b) The same site potential distribution as in panel (a) but visualized on a Petrie polygon of the given 4D hypercube.

where the symbol \dagger denotes the Hermitian conjugation operation [51]. This chirality ensures that the eigenvalues of the matrix H_n (H'_n) have the mirror reflection symmetry with respect to a mean eigenvalue (a zero of the energy) [29]. The chiral symmetry is, in general, broken, that is $\mathcal{C}\psi_{\lambda_k} \equiv \psi_{\lambda_{N-1-k}}$, for ordered eigenvalues $\lambda_0 < \dots < \lambda_{N-1}$. Though, non-degenerate zero-energy states of H'_n , if any, respect the the chiral symmetry of the system [52].

To illustrate the described construction of a hypercube with a simple example, let us consider the 4D case. Specifically, we assign the following values to the diagonal elements of each dion Hamiltonian matrix S_k in Eq. (7), $k = 1, \dots, 4$: $\beta_k = -\alpha_k = -\sqrt{k}$, which guarantees that the on-site potentials of the resulting hypercube with H_4 are incommensurate. To visualize the obtained 4D-

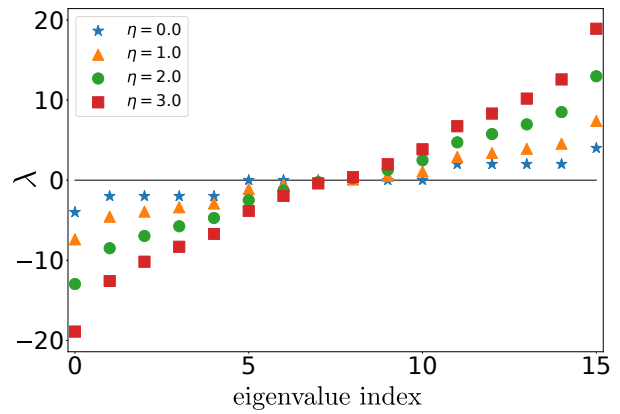


FIG. 2. Eigenvalues λ of the Hamiltonian H_4 describing a 4D hypercube. The matrix H_4 is constructed according to Eq. (7) with elements of the dion matrices S_k taken as $\alpha_k = -\beta_k = \eta\sqrt{k}$, for $k = 1, 2, \dots, 4$, and where the constant parameter η can acquire various values in the range $[0, 1, 2, 3]$.

hypercube with given site potentials, we project it onto the 2D Petrie polygon, as shown in Fig. 1 [53]. Generally, a hypercube with commensurate site potentials produces a degenerate energy spectrum, whereas incommensurate site potentials lift this degeneracy (see also Fig. 2 and the text below).

IV. ENGINEERING COMPACT LOCALIZED STATES

Elaborating on the method described above, we now show how to construct CLSs on hypercubes with sites that have constant potentials. Without loss of generality, we assume that the constant potential is zero ($\alpha_k = \beta_k = 0 \forall k$). For an arbitrary n -dimensional hypercube, the zero potential always results in a highly degenerate spectrum, reminiscent to that observed in flat-band systems but in reciprocal space [18]. However, it is only for even $(2n)$ -dimensional hypercubes that this flat spectrum contains a zero-energy level, which, moreover, has a degeneracy of the degree $m_{2n} = (2n)!/(n!)^2$ [48].

For instance, in the case of the 8D hypercube with $2^8 = 256$ vertices and $2^7 \cdot 8 = 1024$ edges, the degeneracy of the zero-energy level is $m_8 = 8!/(4!)^2 = 70$ [see also Fig. 3(b)]. Furthermore, these degenerate ZESs, denoted as ψ_0^k , $k = 1, \dots, m_{2n}$, are *extended* in nature, i.e., with site amplitudes equal $\psi_0^k(i) \equiv \pm 1$ [54], and which form the orthogonal basis. Because of this, any superposition

$$\psi_0^s \equiv \sum_k c_k \psi_0^k, \quad c_k \in \mathbb{C}, \quad (15)$$

is also a ZES. Interestingly, some superpositions in Eq. (15) can result in *destructive interference, leading thus to the formation and coexistence of the CLSs*, where only a fraction of the sites have nonzero amplitudes [18]. We plot one of the realizations of such CLSs in Fig. 3. As

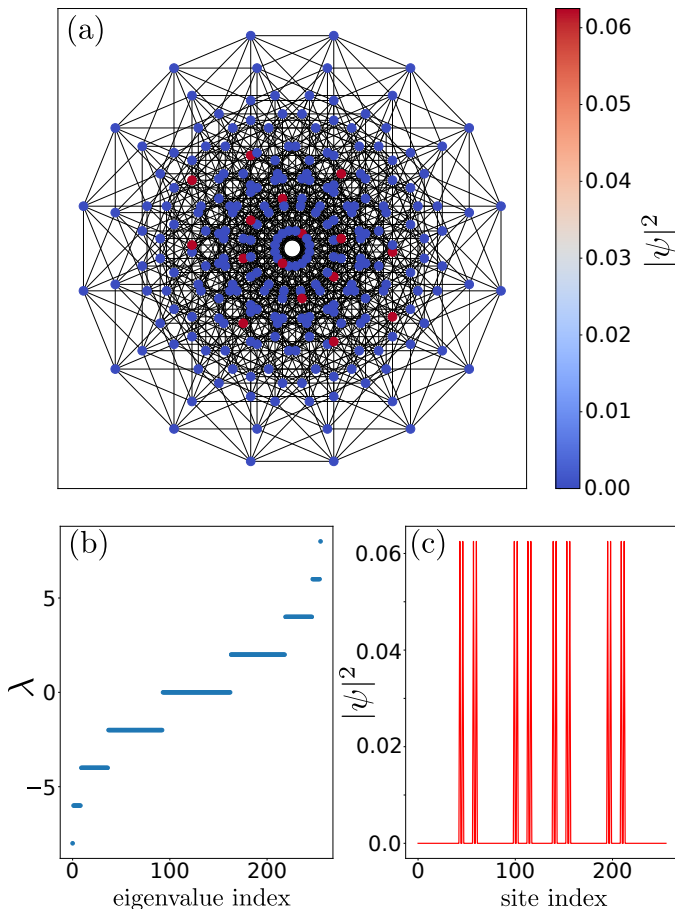


FIG. 3. (a) The intensity of a zero-energy compact localized state (CLS) of an 8D hypercube with zero site potentials visualized on a hypercube Petrie polygon. (b) The degenerate ‘flat band’ energy spectrum of the given hypercube Hamiltonian H_8 . (c) Similar to panel (a) showing the CLS intensity distribution as a function of the site index.

can be seen from the graph, there are only a few nonzero peaks in the CLS, whereas other sites have strictly zero amplitude. Clearly, one can also find such a similarity transformation (a permutation matrix) for the Hamiltonian H_8 which will position all these nonzero peaks next to each other [22].

Note that the Hamiltonian of an n -dimensional bosonic hypercube graph in Eq. (2) with everywhere $\nu(i) = 0$, apart from the chiral symmetry, also respects parity symmetry, meaning that $H_n = \mathcal{P}H_n\mathcal{P}$, where the parity operator $\mathcal{P} = \bigotimes_{k=1}^n \sigma_x$, with σ_x being the Pauli matrix. Moreover, the zero-energy degenerate states ψ_0^k share the same parity, implying that the superpositions in Eq. (15) are also eigenstates of the operator \mathcal{P} . Consequently, any perturbations that respect this symmetry will leave such CLSs unchanged.

Regarding chiral symmetry, the degenerate states ψ_0^k may enter the combination in Eq. (15) with opposite chirality; meaning that, in general, a superposition ψ_0^s is not

the eigenstate of the operator \mathcal{C} . However, certain combinations of ψ_0^k may form chiral eigenstates ψ_0^s : $\mathcal{C}\psi_0^s \equiv \psi_0^s$, making them additionally robust against perturbations that respect this symmetry [52].

V. ENGINEERING NON-COMPACT LOCALIZED STATES

Here we discuss the formation of zero-energy NCLSs on hypercubes with both commensurate and incommensurate site potentials. Additionally, we demonstrate how to generate such states with specific localization features.

A ZES of a Hamiltonian H_n describing a n -dimensional hypercube, with varying site potentials in Eq. (8), can always be straightforwardly obtained from Eq. (7) by choosing the parameters of each matrix S_k such that $\beta_k = \alpha_k^{-1}$. This is because S_k has a zero-valued determinant whenever $\alpha_k\beta_k = 1$. The (unnormalized) zero-energy eigenvectors of the S_k reads [55]

$$\psi_{k,\lambda=0} \equiv [\beta_k, 1]^T. \quad (16)$$

For a n -dimensional hypercube, the zero-energy eigenvector, according to Eq. (11), then takes the form

$$\psi_0 = \bigotimes_{k=1}^n \psi_{k,\lambda=0}. \quad (17)$$

Due to the binary-tree structure of the eigenvectors, resulting from the Kronecker product [48], the elements of the resulting eigenstate ψ_0 can be easily encoded with binary strings. Specifically, the binary string consisting of n elements $i = i_1i_2 \dots i_n$, with $i_k = 0, 1$, represents the decimal index i of the site amplitude $\psi_0(i)$. Moreover, this string also encrypts the element $\psi_0(i)$ expressed as

$$\psi_0(i) \equiv \beta_1^{-i_1} \beta_2^{-i_2} \dots \beta_D^{-i_n}, \quad (18)$$

where the notation $\neg i_k$ denotes the NOT operation over the boolean i_k . For instance, take a 3D hypercube or simply a cube. Its zero-energy eigenvector reads

$$\psi_0^{(b)} \equiv \begin{bmatrix} \beta_1\beta_2\beta_3, \beta_1\beta_2, \beta_1\beta_3, \beta_1, \beta_2\beta_3, \beta_2, \beta_3, 1 \\ 000, 001, 010, 011, 100, 101, 110, 111 \end{bmatrix}^T. \quad (19)$$

In Eq. (19), the upper line accounts for the actual elements of the vector ψ_0 , whereas the lower line refers to their binary representation according to Eq. (18).

Based on the structure of the *zero-energy eigenvector* in Eq. (17), one can construct a vector state of a n -dimensional hypercube with desired localization characteristics. Indeed, suppose now that one wishes to obtain a specific zero-energy eigenstate on 8D hypercube. Assume first that the desired ZES is a single-site localized state at

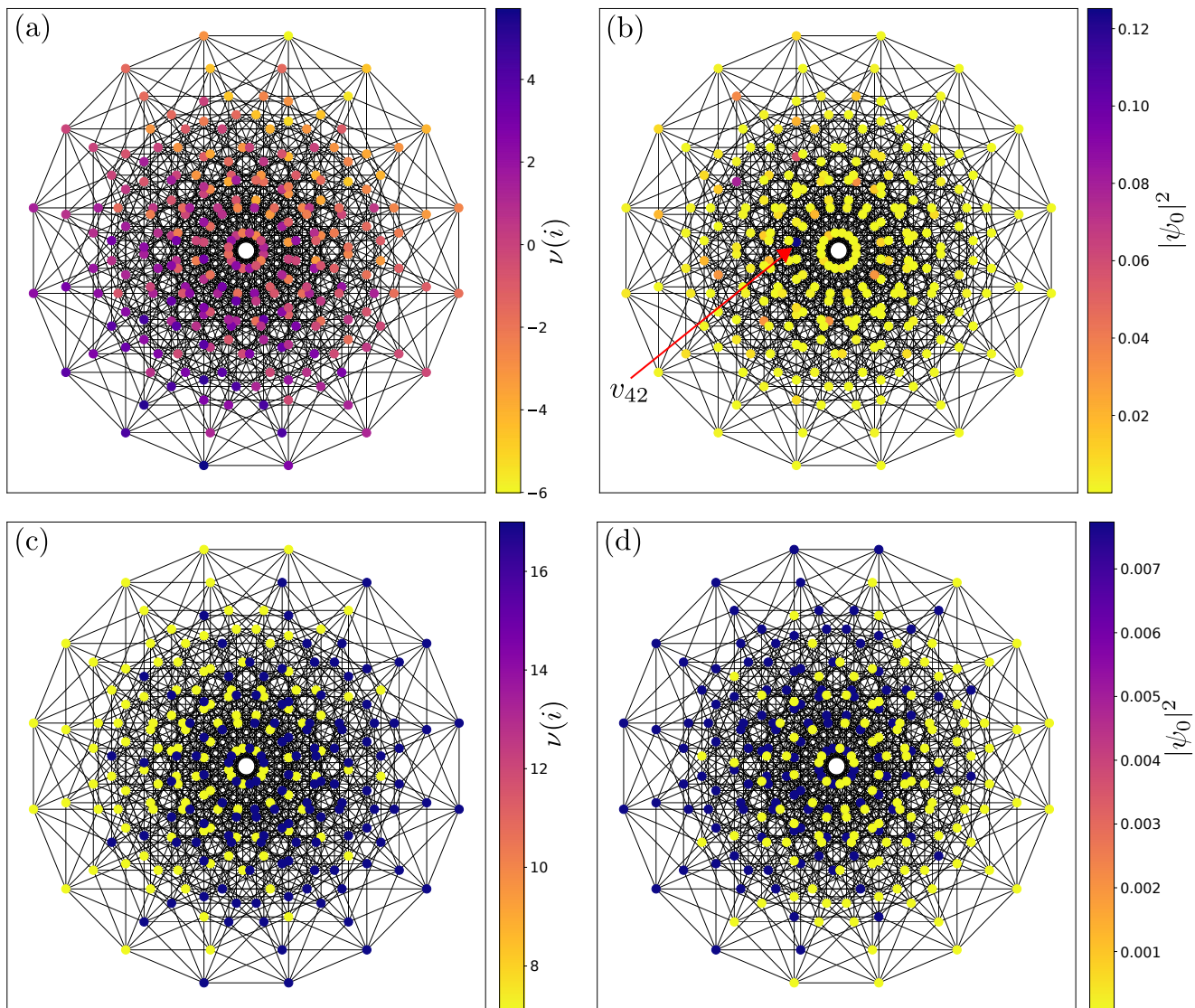


FIG. 4. Panels (a) and (c) show site potential distributions of the 8D hypercube that result in (b) the zero-energy non-compact localized state (NCLS) ψ^{42} , and (d) the domain wall NCLS, respectively.

the vertex say $v(42)$. In the state ψ_0^{42} , the vertex with the index 42, which in the boolean form reads as $b00101010$, has the following amplitude $\psi_0^{42} = \beta_1\beta_2\beta_4\beta_6\beta_8$, according to Eq. (18). To guarantee that the ZES amplitude concentrates at the vertex $v(42)$ one must then ensure that $|\beta_{3,5,7}| \ll 1 < |\beta_{1,2,4,6,8}|$. We plot one of the possible hypercube potential distribution on Fig. 4(a) which generates the localized state shown in Fig. 4(b). We also present complementary plots with the eigenspectrum decomposition for the 8D cube in Fig. 5. From Fig. 5 it is seen that apart from a delta-like peak at the vertex $v(42)$, there is a number of other smaller peaks which correspond to the products of four, three, and so on, terms of β_k in Eq. (18). By varying the values of β_k one can correspondingly modify the intensity of these satellite peaks as desired. It must be noted that the localization

is observed in the whole eigenspectrum, not only for the ZES.

Next, suppose that the intended ZES is a “domain wall” state, meaning that only one half (assume the first half) of the vertices can be excited [56]. This can be readily achieved by having the first half of the elements of the zero-energy vector ψ_0 possess the term β_1 . Note that each term β_k has a vertex periodicity $2^{-k}L$ in ψ_0 , where $L = 2^n$ is the system length, in the considered case $L = 2^8$. By setting $|\beta_1| > 1$, and the rest terms $|\beta_{2,\dots,8}| \approx 1$, one attains an 8D-hypercube with the desired ZES [see Figs. 4(c),(d)]. The explicit form of the spectrum and the density of the domain wall state ψ_0 are also shown in Figs. 5(c),(d). Panels (c) and (d) in Fig. 4 show that vertex excitations in this ZES exhibit a duality with the potential distribution on the hypercube.

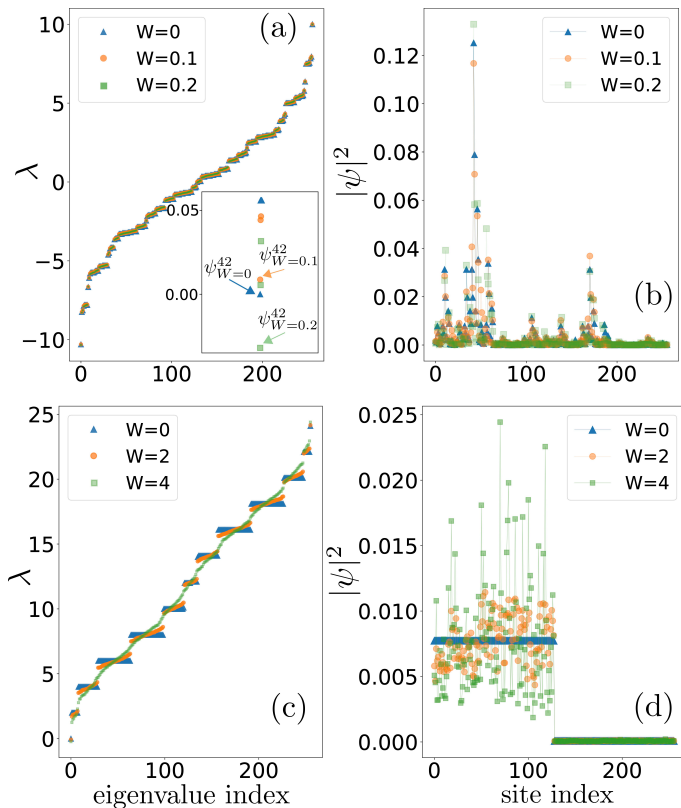


FIG. 5. Energy spectrum and state intensity of the zero-energy localized state ψ^{42} [(a),(b)], and the zero-energy domain wall state [(c),(d)], respectively, using various perturbations drawn from a uniform distribution in the range $[-W, W]$ (see details in the main text). The inset in panel (a) shows the detailed energy spectrum [which is almost overlapped for different values of the parameter W in panel (a)] and corresponding perturbed zero-energy state around the zero-energy level.

Specifically, hypercube sites with smaller potentials (in absolute magnitude) have a higher probability of being excited in this state.

We note that the above ability to engineer hypercube eigenstates with prescribed localization properties allows to emulate genuine *Anderson single-site localized states* on a hypercube subjected to disorder (see also Appendix A).

A. Robustness of the non-compact localized states to perturbations

Given the fact that NCLSs are reminiscent of Anderson states induced by disorder, it is natural to expect that NCLSs are robust to external perturbations. Obviously, perturbations that respect chiral symmetry of the Hamiltonian (within the appropriate gauge) preserve NCLSs. We further study the *robustness* of the 8D hypercube Hamiltonian when the site potentials are perturbed by random values drawn from a uniform distribution over

the range $[-W, W]$, with $W \in \mathbb{R}$.

Two scenarios can be distinguished upon such perturbations: (i) when the density of states near zero energy is high, and (ii) when the ZES is well isolated from the rest of the spectrum.

For the first case, our analysis shows that whenever $W \lesssim |\lambda^e|$, where λ^e is the energy gap, i.e., the distance between the first excited state above or below zero of the unperturbed system, the initial ZES remains immune to perturbations. Namely, despite that the zero energy of the initial state can be shifted, the perturbed ZES remains closest to the zero energy level [see Fig. 5(a),(b)]. However, for larger values of W , the initial ZES, while preserving its shape, can be shifted far away from the level $\lambda = 0$, becoming an excited state [see Fig. 5(a),(b)].

For the second scenario, the ZES exhibits larger robustness against disorder. Namely, the energy of the initial ZES remains zero upon perturbations. However, the modification of the state increases with larger disorder W [see panels (c) and (d) in Fig. 5]. In both scenarios, the increasing values of W eventually leads to the emergence of continuous energy spectra, which is an indicator of a completely disordered system [57] [see Fig. 5].

The above observation implies that a ZES of a hypercube, within a region of the state space with a high (low) density of states, exhibits high (low) susceptibility to perturbations. In other words, isolating the ZES in the system spectrum, allows for the engineering of the robust system response in the presence of disorder. We also note that the ZES also remains immune to purely imaginary perturbations, e.g., when the potentials disorder is dissipative in nature (see Appendix B for details).

VI. CONCLUSIONS AND OUTLOOK

In conclusion, we reveal that localization phenomena can naturally emerge on hypercube bosonic graphs without the presence of disorder, contrary to previous suggestions. Moreover, in parallel we presented a method allowing for engineering various CLSs and NCLSs on such disorder-free hypercubes. Namely, we showed that for the hypercubes with constant site potentials, the resulting highly degenerate energy spectrum in real space enables producing CLSs. Whereas the incommensurate site potentials lead to the emergence of NCLSs with prescribed localization features. Given the importance of CLSs and NCLSs in the realization of various information and wave manipulation protocols, our results can potentially lead to advancements in these fields. The hypercube bosonic graphs presented and their localization properties can be directly simulated in existing experimental photonic platforms exploiting both real and synthetic spaces [44–46].

Additionally, the approach used can be readily extended to other hyperpolytopes constructed by iterative Cartan products of triangles, tetrahedrons, and so on. Consequently, in future research we wish to explore other types of CLSs and NCLSs that can be engineered in these

hyperstructures. In relation to this, it would be also interesting to investigate how the studied localization phenomena on hypercubes are modified when mapped to lower-dimensional systems [29].

ACKNOWLEDGMENTS

I.A. acknowledges support from Air Force Office of Scientific Research (AFOSR) Award No. FA8655-24-1-7376, and from the Ministry of Education, Youth and Sports of the Czech Republic Grant OP JAC No. CZ.02.01.01/00/23_021/0008790. F.N. is supported in part by: Nippon Telegraph and Telephone Corporation (NTT) Research, the Japan Science and Technology Agency (JST) [via the Quantum Leap Flagship Program (Q-LEAP)], and the Moonshot R&D Grant Number JP-MJMS2061], and the Office of Naval Research (ONR) (via Grant No. N62909-23-1-2074).

Appendix A: Emulating disorder-induced Anderson localization on disorder-free hypercubes

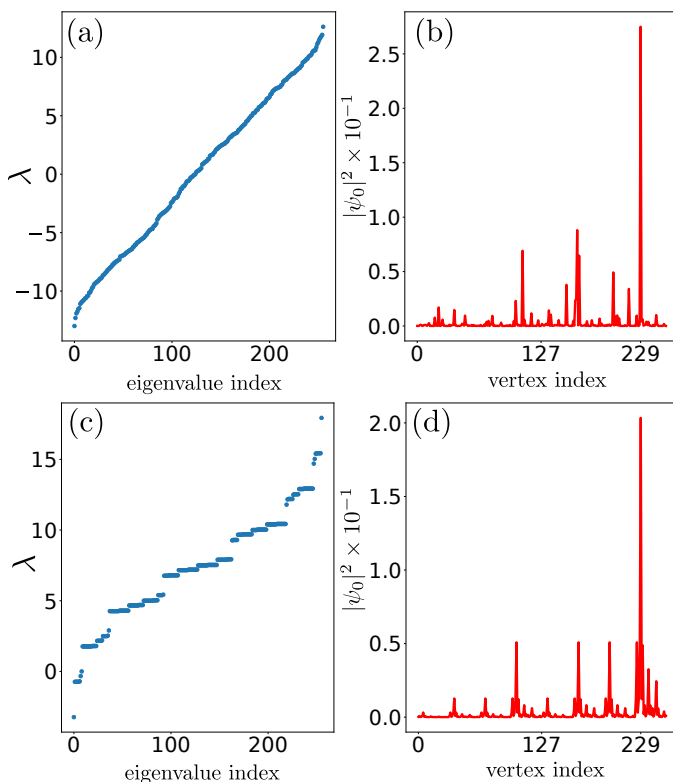


FIG. 6. Energy spectrum (a) and intensity of the localized state that is closest to zero-energy of an 8D hypercube with disorder strength $W = 10$. The energy spectrum (c) and zero-energy localized state intensity of disorder-free 8D hypercube, constructed according to the method described in Sec. V in the main text.

In the main text, we discussed the formation of NCLSs on disorder-free hypercubes. Here we further elaborate on the simulation of disorder-induced Anderson localization on disorder-free hypercube graphs.

For that we first impose disorder on an 8D hypercube, initially characterized by zero on-site potentials, which is drawn from the uniform distribution $[-W, W]$, similar to that in Sec. V A in the main text. For large values $W \gg 0$, the disorder induces Anderson localization. We plot a disorder-induced localized state closest to zero-energy in Fig. 6. As seen in panel (a), the energy spectrum is continuous, indicating the onset of the Anderson localization transition. In panel (b) we show the closest to zero-energy state (ZES) that has localization peaks over a few sites, and with the maximum at the site $v(229)$.

Next, we aim to simulate a similar localized state using a disorder-free hypercube according to the method described in Sec. V. Namely, by identifying the ZES amplitude at the site $v(229)$ as $\psi_0(229) = \beta_4\beta_5\beta_7$, according to Eq. (18), and by setting $|\beta_{4,5,7}| \gg 1$ and $|\beta_{1,2,3,6,8}| \ll 1$, one can easily construct the ZES with similar localization characteristics [compare panels (b) and (d) in Fig. 6], and whose spectrum is still discrete.

Appendix B: Robustness of non-compact localized states under dissipative perturbations

In this section we discuss the robustness of NCLSs against perturbations which are dissipative in nature. We analyze this resilience explicitly in the time evolution of the state.

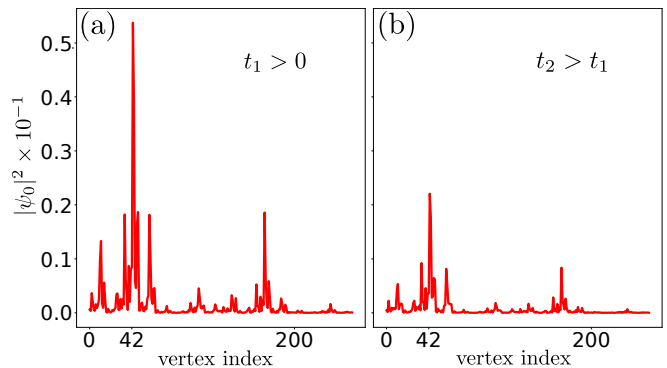


FIG. 7. Time evolution of the NCLS ψ^{42} , initially defined on disorder-free hypercube in Fig. 5(b), subjected to imaginary disorder drawn from the uniform distribution $[0, i]$ at time: (a) $t = 1$, and (b) $t = 2$. The energy and time scale is set by $\kappa = 1$ in Eq. (7)

Indeed, let us now assume that the state dynamics is governed by the time-independent Schrödinger equation, with the (perturbed) Hamiltonian H_n . The hypercube Hamiltonian can describe a network of coupled optical cavities or waveguides with losses, and thus can be written in the matrix mode representation. The solution for

the state dynamics then reads

$$\psi(t) = \exp\left(-iH_n t\right)\psi(0), \quad (\text{B1})$$

where we set the Planck's constant $\hbar = 1$. For the studied 8D hypercube, the Hamiltonian matrix takes the form

$$H_n = H_8 - i\text{diag}[\gamma_1, \dots, \gamma_N], \quad (\text{B2})$$

where H_8 is the Hamiltonian of the unperturbed hyper-

cube in Eq. (7), and the parameters γ_k are sampled from the uniform distribution $[0, W]$. We initialize the system in the zero-energy state ψ^{42} , localized at the vertex $v(42)$ as shown in Figs. 4(b), 5(b), and we set $W = 1$. In this case, the state ψ^{42} still preserves its shape over time, though it begins steadily decaying with a certain rate depending on the disorder strength (see Fig. 7). For larger values $W \gg 1$, the dynamics of the state becomes more intricate due to the growing role of the dissipation eventually leading to the complete loss of the initial state.

-
- [1] P. W. Anderson, "Absence of diffusion in certain random lattices," *Phys. Rev.* **109**, 1492–1505 (1958).
- [2] N. Mott, "The mobility edge since 1967," *J. Phys. C: Solid State Phys.* **20**, 3075 (1987).
- [3] A. Lagendijk, B. van Tiggelen, and D. S. Wiersma, "Fifty years of Anderson localization," *Physics Today* **62**, 24–29 (2009).
- [4] E. Abrahams, *50 years of Anderson localization* (World Scientific, 2010).
- [5] V. Freilikher, Y. Bliokh, K. Y. Bliokh and F. Nori, "Anderson localization of light in layered dielectric structures," in *Optical Properties of Photonic Structures* (CRC Press, 2012) pp. 55–86.
- [6] L. A. Pastur, I. M. Lifshits, S. A. Gredeskul, *Introduction to the Theory of Disordered Systems* (Wiley-VCH, 1988).
- [7] S. Aubry and G. André, "Analyticity breaking and Anderson localization in incommensurate lattices," *Ann. Israel Phys. Soc.* **3**, 18 (1980).
- [8] D. R. Grempel, Shmuel Fishman, and R. E. Prange, "Localization in an incommensurate potential: An exactly solvable model," *Phys. Rev. Lett.* **49**, 833–836 (1982).
- [9] P. Wang, Y. Zheng, X. Chen, *et al.*, "Localization and delocalization of light in photonic Moiré lattices," *Nature* **577**, 42–46 (2019).
- [10] F. Sgrignuoli, R. Wang, F. A. Pinheiro, and L. Dal Negro, "Localization of scattering resonances in aperiodic Vogel spirals," *Phys. Rev. B* **99**, 104202 (2019).
- [11] Z. Zhu, S. Yu, D. Johnstone, and L. Sanchez-Palencia, "Localization and spectral structure in two-dimensional quasicrystal potentials," *Phys. Rev. A* **109**, 013314 (2024).
- [12] B. Freedman, G. Bartal, M. Segev, *et al.*, "Wave and defect dynamics in nonlinear photonic quasicrystals," *Nature* **440**, 1166–1169 (2006).
- [13] Markus Greiner, Olaf Mandel, Tilman Esslinger, Theodor W. Hänsch, and Immanuel Bloch, "Quantum phase transition from a superfluid to a mott insulator in a gas of ultracold atoms," *Nature* **415**, 39–44 (2002).
- [14] Robert Jördens, Niels Strohmaier, Kenneth Günter, Henning Moritz, and Tilman Esslinger, "A mott insulator of fermionic atoms in an optical lattice," *Nature* **455**, 204–207 (2008).
- [15] A. Smith, J. Knolle, D. L. Kovrizhin, and R. Moessner, "Disorder-free localization," *Phys. Rev. Lett.* **118**, 266601 (2017).
- [16] M. Brenes, M. Dalmonte, M. Heyl, and A. Scardicchio, "Many-body localization dynamics from gauge invariance," *Phys. Rev. Lett.* **120**, 030601 (2018).
- [17] N. Chakraborty, M. Heyl, P. Karpov, and R. Moessner, "Disorder-free localization transition in a two-dimensional lattice gauge theory," *Phys. Rev. B* **106**, L060308 (2022).
- [18] F. Nori and Q. Niu, "Angular momentum irreducible representation and destructive quantum interference for Penrose lattice Hamiltonians," *Quasi Crystals and Incommensurate Structures in Condensed Matter* (World Scientific, Singapore, 1990), 434 (1990).
- [19] S. Flach, D. Leykam, J. D. Bodyfelt, P. Matthies, and A. S. Desyatnikov, "Detangling flat bands into Fano lattices," *Europhys. Lett.* **105**, 30001 (2014).
- [20] W. Maimaiti, A. Andreanov, H. C. Park, O. Gendelman, and S. Flach, "Compact localized states and flat-band generators in one dimension," *Phys. Rev. B* **95**, 115135 (2017).
- [21] M. Röntgen, C. V. Morfonios, I. Brouzos, F. K. Diakonov, and P. Schmelcher, "Quantum network transfer and storage with compact localized states induced by local symmetries," *Phys. Rev. Lett.* **123**, 080504 (2019).
- [22] M. Röntgen, C. V. Morfonios, and P. Schmelcher, "Compact localized states and flat bands from local symmetry partitioning," *Phys. Rev. B* **97**, 035161 (2018).
- [23] A. Andreanov, D. Leykam and S. Flach, "Artificial flat band systems: from lattice models to experiments," *Adv. Phys.: X* **3**, 1473052 (2018).
- [24] D. Leykam and S. Flach, "Perspective: Photonic flat bands," *APL Photon.* **3**, 070901 (2018).
- [25] N. Hatano and D. R. Nelson, "Localization transitions in non-Hermitian quantum mechanics," *Phys. Rev. Lett.* **77**, 570–573 (1996).
- [26] N. Hatano and D. R. Nelson, "Vortex pinning and non-Hermitian quantum mechanics," *Phys. Rev. B* **56**, 8651–8673 (1997).
- [27] S. Yao and Z. Wang, "Edge states and topological invariants of non-Hermitian systems," *Phys. Rev. Lett.* **121**, 086803 (2018).
- [28] V. M. Martinez Alvarez, J. E. Barrios Vargas, and L. E. F. Foa Torres, "Non-Hermitian robust edge states in one dimension: Anomalous localization and eigenspace condensation at exceptional points," *Phys. Rev. B* **97**, 121401 (2018).
- [29] I. I. Arkhipov and F. Minganti, "Emergent non-Hermitian localization phenomena in the synthetic space of zero-dimensional bosonic systems," *Phys. Rev. A* **107**, 012202 (2023).
- [30] T. Ozawa, H. M. Price, A. Amo, N. Goldman, M. Hafezi, L. Lu, M. C. Rechtsman, D. Schuster, J. Simon, O. Zilberberg, and I. Carusotto, "Topological photonics," *Rev. Mod. Phys.* **91**, 015006 (2019).

- [31] E. J. Bergholtz, J. C. Budich, and F. K. Kunst, “Exceptional topology of non-Hermitian systems,” *Rev. Mod. Phys.* **93**, 015005 (2021).
- [32] S. Weimann, M. Kremer, Y. Plotnik, Y. Lumer, S. Nolte, K. G. Makris, M. Segev, M. C. Rechtsman, and A. Szameit, “Topologically protected bound states in photonic parity–time-symmetric crystals,” *Nat. Mater.* **16**, 433–438 (2017).
- [33] A. Roy, M. Parto, R. Nehra, C. Leefmans, and A. Marandi, “Topological optical parametric oscillation,” *Nanophotonics* **11**, 1611–1618 (2022).
- [34] S. Weidemann, M. Kremer, T. Helbig, T. Hofmann, A. Stegmaier, M. Greiter, R. Thomale, and A. Szameit, “Topological funneling of light,” *Science* **368**, 311–314 (2020).
- [35] W. König, *The Parabolic Anderson model, Random Walk in Random Potential* (Birkhäuser, Basel, 2016).
- [36] A. Semenov, N. Murphy, S. Patscheider, A. Bernardi, and E. Blokhina, “A quantum implementation of high-order power method for estimating geometric entanglement of pure states,” (2024), [arXiv:2405.19134](https://arxiv.org/abs/2405.19134).
- [37] L. A. Howard, T. J. Weinhold, F. Shahandeh, J. Combes, M. R. Vanner, A. G. White, and M. Ringbauer, “Quantum hypercube states,” *Phys. Rev. Lett.* **123**, 020402 (2019).
- [38] H. Goto, “High-performance fault-tolerant quantum computing with many-hypercube codes,” *Sci. Adv.* **10**, eadp6388 (2024).
- [39] G. Parisi, “D-dimensional arrays of Josephson junctions, spin glasses and q-deformed harmonic oscillators,” *J. Phys. A: Math. Gen.* **27**, 7555 (1994).
- [40] E. Marinari, G. Parisi, and F. Ritort, “Replica theory and large-d josephson junction hypercubic models,” *J. Phys. A: Math. Gen.* **28**, 4481 (1995).
- [41] Y. Jia and J.J.M. Verbaarschot, “Chaos on the hypercube,” *J. High Energ. Phys.* **2020**, 154 (2020).
- [42] L. Avena, O. Gün, and M. Hesse, “The parabolic anderson model on the hypercube,” *Stoch. Process. Their Appl* **130**, 3369–3393 (2020).
- [43] M. Štefaňák and S. Skoupý, “Quantum walk state transfer on a hypercube,” *Phys. Scr.* **98**, 104003 (2023).
- [44] C. Leefmans, A. Dutt, J. Williams, L. Yuan, M. Parto, F. Nori, S. Fan, and A. Marandi, “Topological dissipation in a time-multiplexed photonic resonator network,” *Nat. Phys.* **18**, 442 (2022).
- [45] M. Parto, C. Leefmans, J. Williams, F. Nori, and A. Marandi, “Non-Abelian effects in dissipative photonic topological lattices,” *Nat. Commun.* **14** (2023).
- [46] C.R. Leefmans, M. Parto, J. Williams, *et al.*, “Topological temporally mode-locked laser,” *Nat. Phys.* **20**, 852 (2024).
- [47] H. S. M. Coxeter, *Regular Polytopes* (Dover Publications; 3rd edition, New York, 1973).
- [48] I. I. Arkhipov, A. Miranowicz, F. Nori, Ş. K. Özdemir, and F. Minganti, “Fully solvable finite simplex lattices with open boundaries in arbitrary dimensions,” *Phys. Rev. Res.* **5**, 043092 (2023).
- [49] F. Harary, J. P. Hayes, and H.-J. Wu, “A survey of the theory of hypercube graphs,” *Comput. Math. Appl.* **15**, 277–289 (1988).
- [50] J. Maldacena and X.-L. Qi, “Eternal traversable wormhole,” (2018), [arXiv:1804.00491](https://arxiv.org/abs/1804.00491) [hep-th].
- [51] C.-K. Chiu, J. C. Y. Teo, A. P. Schnyder, and S. Ryu, “Classification of topological quantum matter with symmetries,” *Rev. Mod. Phys.* **88**, 035005 (2016).
- [52] A. Ramachandran, A. Andreanov, and S. Flach, “Chiral flat bands: Existence, engineering, and stability,” *Phys. Rev. B* **96**, 161104 (2017).
- [53] A Petrie polygon for a regular hypercube or any polytope of n dimensions is a skew polygon in which every $(n - 1)$ consecutive sides (but not n) belongs to one of the facets [47, 58].
- [54] Indeed, each matrix S_k in Eq. (7) with $\alpha_k = \beta_k = 0$ has two eigenstates $\psi_1 = [1, 1]^T$ and $\psi_2 = [-1, 1]^T$, corresponding to eigenvalues $\lambda_{1,2} = \pm 1$. As such, the $2n!/[n!]^2$ -folded degenerate ZESs for a given Hamiltonian H_{2n} , are formed by $2n$ -folded Kronecker products of $n!$ number of states ψ_1 and the same number of states ψ_2 .
- [55] The other eigenvector with the eigenvalue $\lambda_k = \alpha_k + \alpha_k^{-1}$ attains the form $\psi_{k,\lambda \neq 0} \equiv [\alpha_k, 1]^T$.
- [56] J.-y. Choi, S. Hild, J. Zeiher, *et al.*, “Exploring the many-body localization transition in two dimensions,” *Science* **352**, 1547–1552 (2016).
- [57] L. A. Pastur, “Spectral properties of disordered systems in the one-body approximation,” *Commun. Math. Phys.* **75**, 179–196 (1980).
- [58] D. R. Nelson and M. Widom, “Symmetry, Landau theory and polytope models of glass,” *Nucl. Phys. B* **240**, 113–139 (1984).